Climate Dynamics manuscript No.
(will be inserted by the editor)

Scaling relations between Atlantic overturning cells

Dynamical consequences of a deep boundary current sustained by turbulent mixing

Anders Levermann · **Juliette Mignot**

Received: date / Accepted: date

Abstract The Atlantic meridional overturning is dominated by two cells which might be associated with North Atlantic Deep Water (NADW) and Antarctic Bottom Water (AABW). On long time scales, both cells require some process which provides potential energy for the flow. While it is still under discussion whether in case of the upper cell (NADW) this energy is provided by turbulent mixing or Southern Ocean surface wind stress, we argue that in case of the bottom cell, turbulent mixing is the main driver.

We exploit the fact that strong mixing between NADW and AABW has been observed in both hemispheres and that on their southward path branches of upper and bottom cells merge along the western boundary. We argue that density differences within the southward branch of the bottom cell, which are necessary to sustain a western boundary current on long time scales, arise mainly from mixing with relatively light water of northern origin.

As a result we obtain scaling relations for the dependence of strength and vertical extent of the bottom water cell on the amount of NADW and the density difference $\Delta\rho_G$ between inflowing AABW from the south and inflowing NADW from the north. The bottom cell's volume transport increases with both the strength of the upper cell and density difference $\Delta\rho_G$. Counter-intuitively, the vertical extent of the bottom cell decreases for increasing volume transport, which might be relevant for the interpretation of paleoclimatic data. The scaling relations are supported by simulations with the coupled climate model CLIMBER-3α which contains a coarse resolution oceanic general circulation model.

Anders Levermann
Earth System Analysis, Potsdam Institute for Climate Impact Research and Institute of Physics, Potsdam University, Potsdam, Germany, E-mail: anders.levermann@pik-potsdam.de

Juliette Mignot
LOCEAN, CNRS-IRD-UPMC, Université Pierre et Marie Curie, Paris, France

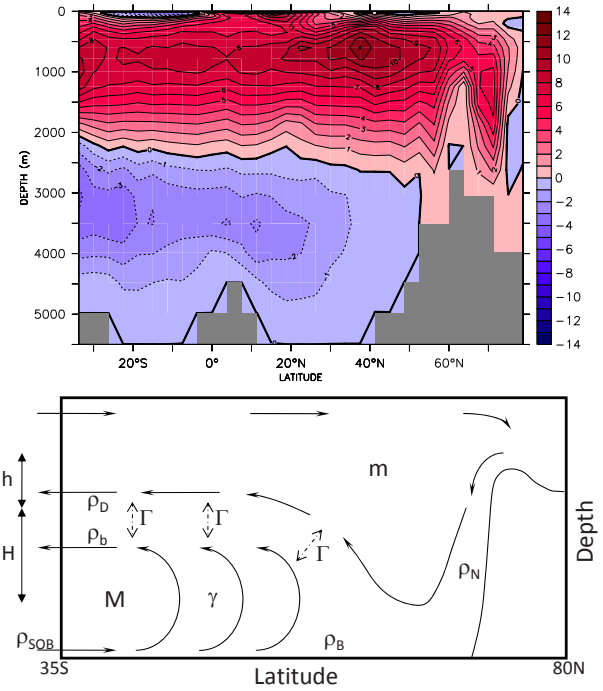

Fig. 1 Zonally averaged view of Atlantic circulation. Panel a: zonally integrated stream function of preindustrial equilibrium of CLIMBER-3α (see appendix B) with contour line differences of 1 Sv $= 10^6 m^3\, s^{-1}$. Panel b: Conceptual configuration for the scaling considerations. Volume transport (solid arrows) advects density in the upper cell (m) and the bottom cell (M). Mixing along the southward flow (Γ) decreases the density of water of Antarctic origin. Mixing within the bottom cell γ creates a density difference between dense inflowing (ρ_{SOB}) and relatively light out-flowing bottom water (ρ_b) and leads to upwelling within the overturning cell. The vertical extent of the cells is denoted by h and H, respectively.

1 Introduction

The abyssal ocean is referred to as the water below the main thermocline, i.e. below a depth of about 1000m. In spite of its huge volume, our general understanding of its circulation remains incomplete. North Atlantic Deep Water (NADW) and Antarctic Bottom Water (AABW) are the dominant water masses of the deep Atlantic circulation. AABW is a cold and fresh water mass of very high density. In the Atlantic Ocean, it is comprised of Weddel Sea Deep Water, which is formed in the Southern Ocean around the Antartic continent, and recirculating lower Circumpolar Deep Water, which enters the Atlantic via the Drake Passage. It circulates below 4000m depth and proceeds on its way northward through a number of deep basins connected by channels through fracture zones at depths of typically 4200m to 4500m. Along its path, it encounters the southward flowing NADW, which is warmer and more saline. The latter is formed in the North Atlantic basin and flows southward below 2000m along the western continental slope. As a result of its higher density, AABW is generally found below NADW.

Interaction between NADW and AABW is crucial for a fundamental understanding of the role and stability of this circulation both in past (Boyle and Keigwin 1982; Curry et al 1988; Rahmstorf 2002) and future climate (Broecker et al 1999; Hattermann and Levermann 2009). The oceanic uptake and transport of nutrients and greenhouse gases are prominently determined by the formation of deep water and its circulation in the different ocean basins (Ganachaud and Wunsch 2002).

Because of its complex path through topography, the core of northward AABW is not generally situated beneath the southward flow of NADW. In particular, Murray and Reason (1999) showed that the existence of deep topographic channels, which are not always properly resolved in models in spite of their considerable impact on motion and temperature of bottom waters, allow AABW to infiltrate basins remote from its source without excessive dilution. Still, observations show that through mixing, AABW is a major contributor to lower NADW (Luyten et al 1993) shifting it towards higher density as it moves southward in the South Atlantic (Reid 1989). Similarly AABW is reported to become warmer and more saline on its path northward (Sloyan and Rintoul 2000) and strong mixing of the two in the Brazil Basin (Sloyan and Rintoul 2000), around the equator (Rhein et al 1998) and in the western North Atlantic (Mauritzen et al 2002) has been observed.

Almost 30 years ago, Whitehead and Worthington (1982) noted that water of Antarctic origin is modified by mixing with North Atlantic Deep Water already well south of the equator. Similarly, properties of NADW formed in northern high latitudes are constantly evolving along their path and one should thus use the terms AABW and NADW with care. However, in a latitude-depth view of the flow field, one can clearly distinguish two overturning cells in the deep Atlantic: the waters of Antarctic origin (AABW) flowing northward along the bottom and returning southward roughly between 2500 and 4000m depth, and the waters of North Atlantic origin, sinking in high northern latitudes and propagating southward around 1000-2500m depth. In this paper, we will deviate from the notation of the majority of observational literature by denoting NADW only the southward branch of the upper overturning cell, i.e. the water of North Atlantic origin. We will use the term AABW to refer to the bottom waters entering the Atlantic from the south. The southward branch of the bottom overturning cell, does not have a clear notation in this paper but we will not refer to it as NADW nor lower NADW even though this is often done in observational literature. The reason is that for the discussion in this paper it is important to distinguish the two cells by their origin as opposed to their properties.

Both proxy data (Adkins et al 2002) and modeling results (Ganopolski et al 1998; Kitoh et al 2001; Hewitt et al 2001; Shin et al 2003; Otto-Bliesner et al 2007) suggest that during the last glacial maximum, NADW was shallower and that the vertical extent of the bottom cell in the Atlantic basin was larger than at present. While the formation of AABW near the Antarctic coast seems to have been rather constant (Duplessy et al 1988; Broecker et al 1990), it remains unclear how AABW was distributed to the ocean basins. In particular, no information exists on the relative strength of Atlantic and Indo-Pacific AABW. Concerning present climate, first attempts to investigate variability of AABW flow into the Atlantic from data (e.g. (Hall et al 1997) and (Limeburner et al 2005)) do not allow to draw clear conclusions for longer timescales.

Using forced oceanic general circulation models (OGCM), Goodman (1998) and Brix and Gerdes (2003) linked global AABW to NADW via an interaction with the Antarctic Circumpolar Current (ACC). England (1993) suggested that the interbasin exchange of NADW is controlled by AABW. Kamenkovich and Goodman (2000) examined the sensitivity to vertical diffusivity specifically for AABW entering the Atlantic. In their theoretical interpretation of the simulations they used the ad-hoc assumption that a shoaling of the upper cell is accompanied by an increase in vertical extent of the bottom cell, such that the sum of the vertical extent of both cells is constant. They found that both cells increased in strength for increasing vertical diffusivity, while the vertical extent of the bottom cell decreased.

Here we propose that mixing with NADW provides the energy source to sustain the Atlantic bottom overturning cell (section 2). On this basis and the assumption that the return flow of the overturning cells is predominately a western boundary current, we derive scaling relations that link strength and vertical extent of the Atlantic bottom cell to the

strength of NADW (section 3). Note that this study does not tackle the mechanisms of AABW production nor that of the global strength of AABW, but merely addresses the question of how much AABW of a given density can sustain a bottom overturning cell in the Atlantic. In section 4, the scaling relations are compared to simulations with the coupled ocean-atmosphere-sea-ice model of intermediate complexity CLIMBER-3α, which contains an oceanic general circulation model with 3.75° horizontal resolution and 24 vertical levels. A detailed description of the model is given in appendix B and by Montoya et al (2005). Sensitivity experiments with respect to Southern Ocean wind stress (Schewe and Levermann 2009), vertical diffusivity (Mignot et al 2006), Atlantic surface freshwater flux (Levermann et al 2005) and atmospheric CO_2 concentrations (Levermann et al 2007) have been carried out as well as an integration with glacial boundary conditions (Montoya and Levermann 2008)

2 Energy source for sustaining the bottom cell

From an energetic perspective it is clear that a deep meridional overturning circulation can only be sustained if some process provides the necessary potential energy for the upwelling within the cell (Sandström 1908; Kuhlbrodt 2008). Otherwise the deep ocean would fill up with dense water (through, for example, deep water formation processes in the Nordic Seas or around Antarctica) without an energetic reason for the water to upwell and close the overturning loop. This concept has been widely accepted for the upper cell of NADW. It is however equally true for the bottom cell (Kuhlbrodt et al 2007).

The upper cell in the Atlantic is in direct contact with the ocean surface. Thus atmospheric fluxes play a dominant role in determining its properties. Whether potential energy is predominantely provided by turbulent mixing (Munk and Wunsch 1998; Wunsch and Ferrari 2004) or the large-scale divergence of Southern Ocean winds in combination with topographic feature of Drake Passage (Toggweiler and Samuels 1998) is still under debate (Kuhlbrodt et al 2007).

The bottom cell is lacking such atmospheric forcing. Still, density gradients are necessary to maintain the flow. On the bases of observations as described in the introduction, we argue here that the necessary energy to sustain the bottom cell is provided by mixing with surrounding water, in particular water of North Atlantic origin. In other words, mixing provides the buoyancy necessary for the waters of Antarctic origin to upwell along their Atlantic path.

While the northward flow of AABW in the Atlantic is confined to bottom topography, the southward branch of the bottom cell returns mainly above topographic features. Observations show that together with the southward branch of the upper (NADW) cell it flows predominately as a western boundary current (WBC) (Molinari et al (1992); Smethie et al (2000); Weatherly et al (2000), figure 2). - a fact that we will use to derive scaling relations between the two cells. In section 3, we will thus mainly exploit the following two assumptions:

1. Energy to sustain the bottom overturning cell in the Atlantic is provided through mixing with NADW
2. NADW and the southward branch of the bottom cell form a deep Western Boundary Current in most of the Atlantic basin

Both statements are based on observations as we argued in the introduction. Though mixing between AABW and NADW has been reported in the whole Atlantic it is not necessarily stongest along the western boundary (Rhein et al 1998; Sloyan and Rintoul 2000; Mauritzen et al 2002). Note that it is not necessary for the upcoming scaling relations that mixing takes place everywhere within the return flow of the bottom cell. We will assume, however, that mixing is stronger for increased inflow of either of the two water masses, NADW and AABW.

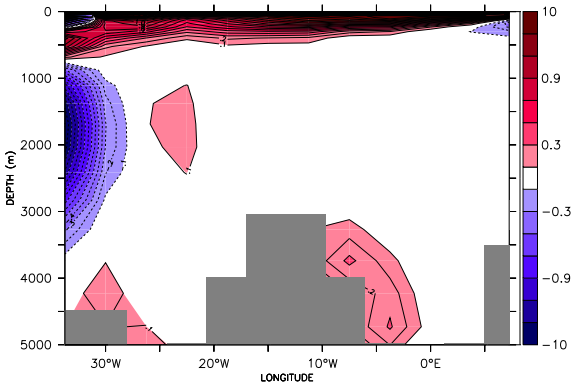

Fig. 2 Zonal cross-section of the northward velocity field at 20°S of pre-industrial equilibrium simulation of CLIMBER-3α (red depicts northward and blue southward flow, the contour level difference is $0.1 cm\,s^{-1}$). NADW and the return branch of the bottom cell flow southward in a WBC.

3 Scaling relations

Figure 1b depicts the conceptual configuration that is meant to mimic interaction of the two overturning cells and that is the basis for the following scaling arguments. Volume transport of the upper cell is denoted by m and that of the bottom cell by M. The dominant physical processes included are the advection of density by the cells as well as mixing within the bottom cell and between both overturning cells. Note that for the sake of clarity we neglect diapycnal mixing within the NADW cell. Observations show that vertical mixing in the pycnocline is indeed small in the Atlantic

(Moum and Osborn 1986; Ledwell et al 1993; Oakey et al 1994; Gregg et al 2003). Consequently the corresponding upwelling within the Atlantic basin should be small.

3.1 Scaling relations for the bottom cell

In the following we will explore the two hypothesis phrased in section 2. Near the western boundary the momentum balance equation reduces to

$$\mu \cdot \rho_0 \cdot \partial_x^2 v = \partial_y p,$$

where μ and $\rho_0 \equiv 10^3\ kg \cdot m^{-3}$ are eddy viscosity and reference density of the ocean, respectively. p denotes the pressure and v the meridional velocity. Integration over a vertical plane crossing the southward branch of the bottom cell at, say 35°S, yields a scaling for its volume transport

$$M = \frac{D^3 \cdot H}{\mu \cdot \rho_0} \cdot \partial_y p$$

where H is the vertical extent of the bottom return flow and $D = (\mu/\beta)^{1/3}$, the width of the frictional boundary layer, is given by eddy viscosity and the north-south gradient of the Coriolis parameter β (Munk 1950). In the horizontal plane at the center of the overturning cell, the meridional pressure gradient vanishes consistent with the absence of a meridional flow. We can therefore relate the meridional pressure gradient to the mean density gradient through $\partial_y p = g \cdot H \cdot \partial_y \rho$, where g is given by gravity. The corresponding scaling yields

$$M = K \cdot H^2 \cdot (\rho_B - \rho_b) \tag{1}$$

with $K \equiv g/(\beta \rho_0 L)$ and L the meridional extent of the bottom cell. ρ_B and ρ_b denote the densities at the northern and southern end of the southward branch of the bottom cell (figure 1b). Similar equations have been obtained in the framework of boundary layer theory (Munk 1950) and have been used in zonally averaged ocean models (Wright et al 1998) as well as conceptual models of the overturning (Stommel 1961; Rahmstorf 1996; Gnanadesikan 1999).

Further scaling can be obtained from the vertical density balance within the bottom cell. Near the ocean bottom, vertical mixing of temperature and salinity is enhanced due to rough topography and reduced stratification (Toole et al 1994; Polzin et al 1997; Ledwell et al 2000; Moum et al 2002). In equilibrium the downward buoyancy transport by mixing within the cell has to be balanced by upward advection. Thus integration of the tracer equation along a horizontal plane in the center of the bottom cell yields a second expression for the volume transport M

$$\delta\rho_0 \cdot M = \gamma \cdot \frac{\rho_{SOB} - \rho_b}{H} \tag{2}$$

We give a detailed derivation of this relation in appendix A. Note that we are aware that the northward inflow of AABW into the Atlantic and the southward return flow along the western boundary do not lie on top of each other (figure 2). Yet, despite the complicated path of AABW along bottom topography, observations show strong mixing between the two water masses (section 1). Similar expressions were used by Kamenkovich and Goodman (2000) for the bottom cell and for mixing through the pycnocline by Gnanadesikan (1999). In this advection-diffusion balance, ρ_{SOB} denotes the density of the inflowing AABW (compare figure 1b), $\gamma = \kappa \cdot L \cdot D$ is a constant given by geometry and the vertical mixing coefficient κ; $\delta\rho_0$ is the scale of a vertical density difference. From the density balance equation for the inflowing branch of AABW we find immediately that $\rho_{SOB} - \rho_B = \delta\rho_0$ which eliminates ρ_B from the problem.

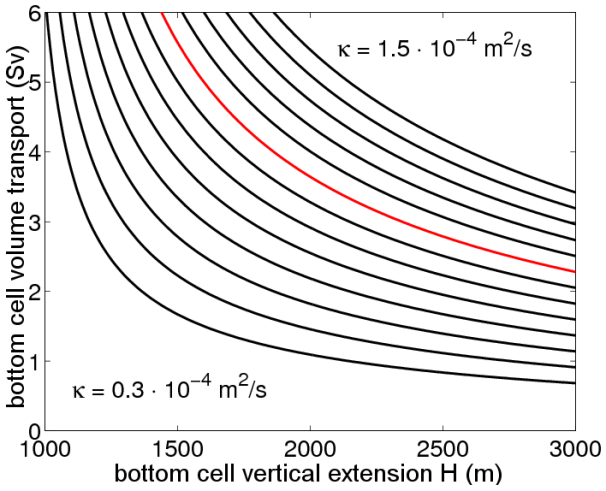

Fig. 3 Volume transport of Atlantic reverse bottom overturning cell as a function of its vertical extent for different values of the vertical diffusivity (κ increases in steps of $0.1 \cdot 10^{-4}\ m^2\ s^{-1}$). A direct consequence of the southward flow being a WBC in most of the Atlantic basin that obeys a vertical balance of advection and diffusion is that the volume transport of the bottom cell decreases with increasing vertical extent. Numerical values are obtained by comparison with the simulations in section 4 and are given in table 1. The red curve corresponds to the value $\kappa = 10^{-4}\ m^2\ s^{-1}$ used for comparison with the simulations in section 4.

Thus the assumption that the return flow of the bottom cell is predominantely a WBC (equation 1) in vertical advection-diffusion balance (equation 2) leads to an expression for its volume transport as a function of its vertical extent

$$M = \frac{\gamma}{H} \cdot \frac{H^3}{H^3 - H_0^3} \tag{3}$$

Figure 3 shows M as a function of H for different values of vertical diffusivity κ. In contrast to a WBC with negligible upwelling within the cell, vertical extent of the bottom cell decreases with increasing volume transport. Note that, from equation (3), H is bound from below and can not be smaller than $H_0 \equiv (\gamma/(K \cdot \delta\rho_0))^{1/3}$, i.e. a minimum extent

of the bottom cell is imposed by the assumptions made in section 2.

3.2 Scaling relations between the cells

The existence of a sustained bottom overturning cell demands the existence of a process that transforms the in-flowing dense bottom water ρ_{SOB} into lighter out-flowing water of density ρ_b. As we argued on the basis of observations in section 2 the necessary potential energy is provided predominantly by density exchange between the southward flowing branch of the two cells (McCartney and Talley 1984; Rhein et al 1998; Sloyan and Rintoul 2000; Laurent et al 2001). The exchange is determined by their mutual density difference $\Delta\rho \equiv \rho_b - \rho_D$ and the mixing coefficient $\Gamma = \kappa \cdot L \cdot D/\delta$ where δ is the penetration depth of the mixing. The corresponding equation is obtained through the density balance from the tracer equation of the southward flowing branch of the bottom cell

$$\Gamma \cdot \Delta\rho = M \cdot (\rho_B - \rho_b) + \gamma \cdot \frac{\rho_{SOB} - \rho_b}{H} \tag{4}$$

The diffusive mass flux between the two overturning cells $\Gamma \cdot \Delta\rho$ has to be balanced by advective (first term on the right) and diffusive (second term on the right) mass flux within the cell. Inserting equations (1) and (2) into the density balance (4) yields the exchange equation

$$\Gamma \cdot \Delta\rho = \frac{M^2}{K \cdot H^2} + M\delta\rho_0 \tag{5}$$

Together with equation (3), it describes the bottom cell as a function of its difference in density to NADW ($\Delta\rho$). Through the diffusion term $\Gamma \cdot \Delta\rho$, AABW becomes lighter along its path in the Atlantic, because dense water is mixed into NADW. In equilibrium, this density gain of NADW has to be balanced by advection within the NADW cell $\Gamma \cdot \Delta\rho = m \cdot (\rho_D - \rho_N)$ where ρ_N is the density of the water mass entering the Atlantic basin from the north (compare figure 1b). Inserting this equation into expression (5) yields an intrinsic equation for the vertical extent H as a function of the NADW volume transport and the external density difference $\Delta\rho_G \equiv \rho_{SOB} - \rho_N$ between the inflowing water masses

$$m \cdot \Delta\rho_G = \left(M \cdot \frac{m+\Gamma}{\Gamma} + m \right) \cdot \frac{M \cdot H}{K \cdot H_0^3} \tag{6}$$

where $M = M(H)$ is taken from equation (3). Equation (6) is the central scaling relation. It is an intrinsic equation for H as a function of the volume transport of NADW m and the density difference between the inflowing water masses $\Delta\rho_G$. Through equation (3) we obtain a solution for the volume transport of the bottom cell M. The three parameters K, H_0 and Γ are given by geometry and the vertical mixing coefficient.

3.3 Structure of solutions

Let us discuss the structure of solutions of equation (6) by considering two idealized situations in which one of the two external quantities, m and $\Delta\rho_G$, are kept constant, respectively. The upper panel of figure 4 shows solutions of equation (6) for different fixed values of NADW volume transport m. An increase in $\Delta\rho_G$ enhances $\Delta\rho$ and thus the diffusive buoyancy flux between the cells. Consequently, volume transport of the bottom cell intensifies with increasing $\Delta\rho_G$. In its lower panel figure 4 shows the solutions for constant $\Delta\rho_G$. With increasing strength of the upper cell m, volume transport of the bottom cell also intensifies. This is due to the fact that the meridional density gradient within the bottom cell is increased through enhanced mixing with NADW.

This process is saturated in the limit of strong NADW ($m \to \infty$). In this case of infinite advection, NADW indeed reaches it lowest density, namely that of the inflowing water mass ρ_N. Using the governing equation (6) and the relation (3) we can derive an intrinsic expression for this saturation curve $M_\infty = M_\infty(\Delta\rho_G) \equiv \lim_{(m\to\infty)} M$

$$\left(\frac{M_\infty (M_\infty + \Gamma)}{\Gamma K H_0^3 \Delta\rho_G} \right)^3 = \frac{\Gamma\Delta\rho_G - (M_\infty + \Gamma)\delta\rho_0}{\Gamma\Delta\rho_G H_0^3} \tag{7}$$

which is given as the red curve in the upper panel of figure 4. For very strong mixing between the overturning cells ($\Gamma \to \infty$), we can derive an upper bound for the saturation value $M^\infty = M^\infty(m) \equiv \lim_{(\Gamma\to\infty)} M$ analytically. In this limit Equation (6) becomes

$$m \cdot \Delta\rho_G = (M^\infty + m) \cdot \frac{M^\infty \cdot H^\infty}{K \cdot H_0^3} \tag{8}$$

which can be solved for $m \to \infty$ using equation (3)

$$M_\infty^\infty = \left(\frac{\Delta\rho_G - \delta\rho_0}{\Delta\rho_G} \right)^{1/3} K \cdot H_0^2 \cdot \Delta\rho_G \tag{9}$$

$$H_\infty^\infty = \left(\frac{\Delta\rho_G}{\Delta\rho_G - \delta\rho_0} \right)^{1/3} H_0 \tag{10}$$

$M_\infty^\infty \equiv \lim_{(\Gamma,m\to\infty)} M$ and $H_\infty^\infty \equiv \lim_{(\Gamma,m\to\infty)} H$ represent absolute upper and lower bounds for M and H, respectively, because of the assumption of infinitely strong mixing.

Note that obviously, both m and $\Delta\rho_G$ might vary simultaneously. The solution structure discussed in figure 4 relate only to idealized situations where one of the two quantities is kept fixed or one is dominating the other.

4 Comparison with climate model simulations

As a simple illustration for the scaling relations, we apply anomalous freshwater flux to the ocean surface in the North Atlantic in CLIMBER-3α, in order to obtain equilibria with different strength of NADW overturning (for details see appendix B). The model applies a second order moment tracer

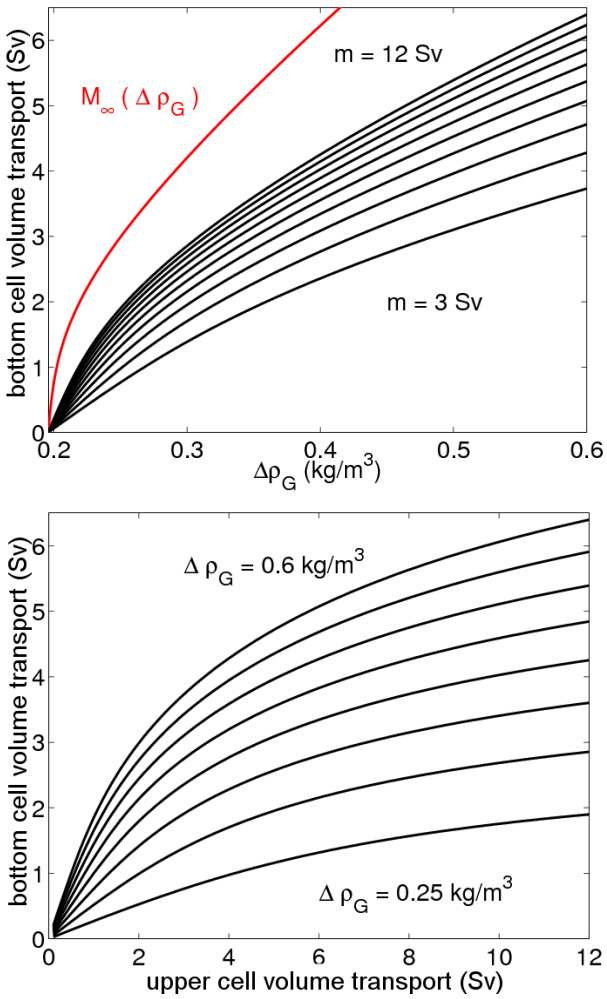

Fig. 4 Solutions of the governing equation (6) for different values of fixed upper cell strength m (upper panel) and for different values of fixed density difference between the inflowing water masses $\Delta\rho_G$ (lower panel). Consistent with the physical mechanism at play AABW volume transport increases with increasing density difference between the inflowing water masses $\Delta\rho_G$. For constant density difference, the volume transports of AABW in the Atlantic varies along with that of NADW. In the limit of strong NADW a saturation is reached (red curve in upper panel). The saturation values of M and H depend only on the mixing coefficient and geometry. For numerical values of the parameters see table 1.

$\Delta\rho_G = 0.4\ kg\cdot m^{-3}$
$\Delta\rho_m = 0.4\ kg\cdot m^{-3}$
$\delta\rho_0 = 0.22\ kg\cdot m^{-3}$
$\kappa = 10^{-4}\ m^2\cdot s^{-1}$
$\beta = 10^{-10}/6\ m^{-1}\cdot s^{-1}$
$\delta = 100\ m$
$D = 2.25\cdot 10^6\ m$
$L = 2\cdot 10^7\ m$
$k = 120\cdot m^4\ kg^{-1}\ s^{-1}$

Table 1 Numerical values for the solution shown in figures 5, 6 and 7.

advection scheme (Prather 1986) which has negligible numerical diffusivity (Hofmann and Maqueda 2006). The low background value of vertical diffusivity used of $\kappa = 0.1\cdot 10^{-4} m^2 s^{-1}$ is consistent with observations in the ocean interior (Ledwell et al 1998) and results in $\sim$3 Sv of upwelling through the pycnocline in the Atlantic (Mignot et al 2006). The model thus reproduces the assumptions used to derive the scaling relations that upwelling within the main pycnocline of the Atlantic is negligible . The effect of enhanced mixing over rough topography and in regions of decreased stratification is parameterized following (Hasumi and Sugihara 1999). This leads to averaged vertical diffusivities of $\kappa = 0.1\cdot 10^{-4} m^2 s^{-1}$ at about 1000m depth, $\kappa = 0.2\cdot 10^{-4} m^2 s^{-1}$ at about 2000m depth and $\kappa = 0.6\cdot 10^{-4} m^2\ s^{-1}$ at about 3000m depth. This increase of vertical mixing with depth, which might be even more pronounced in the real ocean, supports the assumption of section 3 that diapycnal mixing is negligible in the pycnocline but has to be taken into account for the bottom cell.

Figure 5 shows the volume transport of the bottom cell M as a function of the strength of the upper cell m. The simulations show that M weakens along with m. This is consistent with the scaling for constant density difference $\Delta\rho_G$ (figure 4b). Due to the anomalous freshwater flux to the North Atlantic it can be expected that the density difference $\Delta\rho_G = \rho_{SOB} - \rho_N$ increases, which would tend to strengthen M. Thus this effect competes with the weakening effect for M due to weakened NADW. The simulation results in figure 5 suggest a dominance of the influence of the NADW strength m over the influence of the density difference $\Delta\rho_G$. For comparison the solid line provides a solution of the central scaling relation (6) for constant $\Delta\rho_G = 0.4\ kg\ m^{-3}$, using parameter values of table 1. The dashed line gives the corresponding saturation value $M_\infty = 6.2$ Sv for large values of m for the specific parameter choice. It is bound from above by the analytically derived $M_\infty^\infty = 7.1\ Sv$ from equation (9).

Figure 6 shows the numerical solution for the vertical extent H of the bottom cell, which decreases with increasing NADW strength m both as a result of the scaling and in the simulations. The characteristic monotonous decline saturates at $H_\infty = 1154\ m$ which compares well with the lower bound $H_\infty^\infty = 1148\ m$ derived above for infinitely strong m. Note that the limit values M_∞ and H_∞ are completely determined by the external density difference $\Delta\rho_G$ which might vary in the simulations and naturally in the real ocean. This might be specifically important for paleoclimatic situations for which limited information is available.

With respect to vertical extent, the two overturning cells exhibit qualitatively different behaviour. Figure 7 shows the vertical extent h of the upper cell as a function of its volume transport m (black dots). Contrary to the bottom cell (equation (3)), h increases with m in our simulations. The fundamental difference to the bottom cell lies in the absence

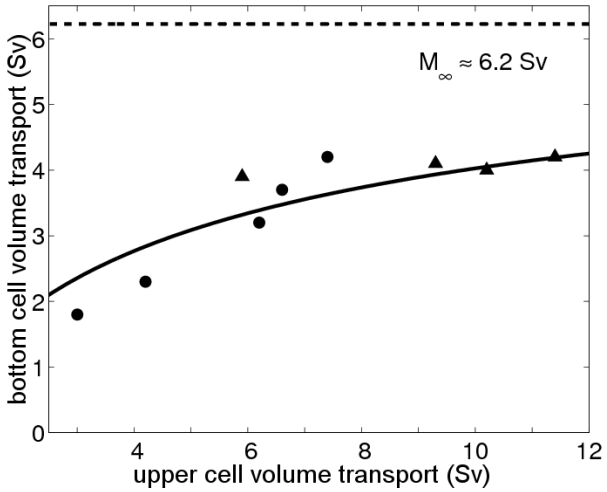

Fig. 5 Theoretical prediction and model simulations: Volume transport M of the bottom Atlantic cell as a function of that of the upper cell m. Both overturning cells strengthen together, but the bottom cell strength saturates for strong upper cell at $M_\infty = 6.2$ Sv.

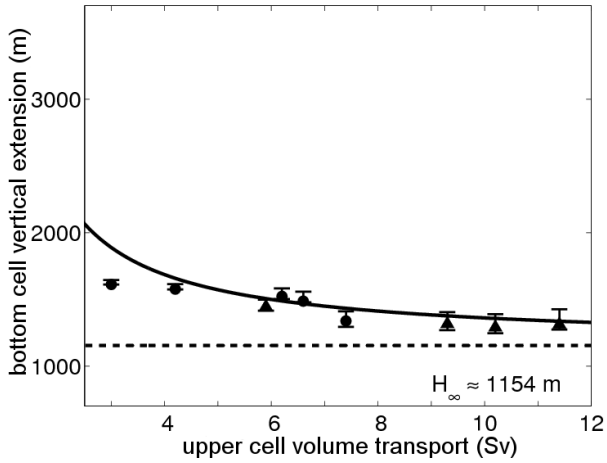

Fig. 6 Vertical extent of the bottom cell H as a function of upper strength m. Though Atlantic bottom cell strength increases with m, its vertical extent decreases. It saturates at $H_\infty = 1126$ m. The definition of H and its error bars is detailed in appendix B.

of strong mixing-driven upwelling of NADW across the Atlantic pycnocline. Since NADW flows as a WBC in most of the basin, m and h are related through the meridional density difference $\Delta\rho_m$ between its northern and southern ends by $m = k \cdot h^2 \cdot \Delta\rho_m$ (Analogue to equation (1) for the bottom cell). The simulation results in figure 7 are consistent with a constant meridional density difference $\Delta\rho_m$ above the pycnocline (black curve in figure 7). The red dots and red curve in figure 7 show the overall vertical extent of the southward flowing water $h+H$. Similar to Kamenkovich and Goodman (2000) we find that the sum $h+H$ is relatively constant in our simulations. It is consistent with the scaling of the vertical extent of the bottom cell H under the assumption of NADW being a WBC with little diffusive upwelling within the Atlantic basin and constant $\Delta\rho_G$.

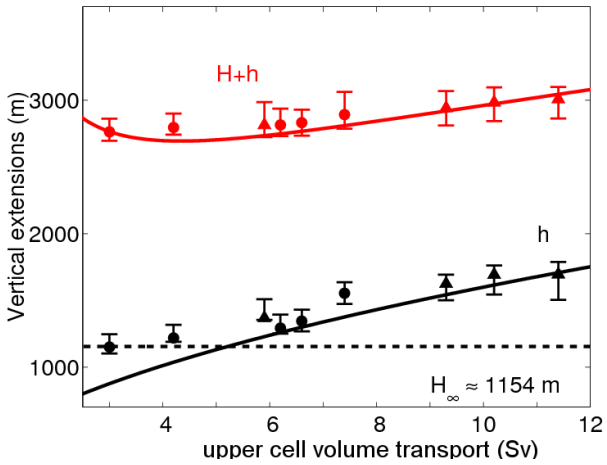

Fig. 7 Vertical extent of southward flowing water masses. The vertical extent of the upper cell increases with its volume transport consistent with low diffusion-driven upwelling within the Atlantic basin. The overall height of southward flowing water masses H+h is approximately constant as previously found by (Kamenkovich and Goodman 2000).

5 Conclusions and Discussion

We propose scaling relations for volume transport and vertical extent of the bottom overturning cell in the Atlantic. The main assumptions are that (1) the potential energy necessary to sustain an overturning cell is provided by turbulent mixing with lighter NADW of northern origin and (2) the bottom cell return flow is predominantly a western boundary current and therefore driven by a meridional density gradient within the cell. Note that this does not imply that AABW is a WBC on its northward path nor does it prohibit strong northward recirculation of the southward flowing waters. Based on these hypotheses which are supported by observations, we derive expressions for the strength and vertical extent of the bottom cell as functions of the volume transport of deep water entering from the north and the external density difference $\Delta\rho_G$ between inflowing AABW and inflowing NADW into the Atlantic.

The scaling is illustrated by comparison with coupled climate simulations. The simulations show an intensification of the bottom cell along with the upper cell and a somewhat counter-intuitive decrease in vertical extent for increasing volume transport of the bottom cell. Both aspects are consistent with the scaling relations in the case where the influence of the upper cell volume transport dominates that of varying $\Delta\rho_G$. This situation is probably dependent on the ex-

perimental set-up. It is however noteworthy that the counter-intuitive decrease in vertical extent of the bottom cell with increasing volume transport on both the upper and bottom cell can be reproduced in a coupled climate model. This inverse behaviour is a direct consequence from the presented scaling and arises from the fact that the bottom cell is in a vertical balance of advection and diffusion. Since a lot of paleoclimatic proxies are rather a measure for the amount of water of a certain origin above the core than of the volume transport of this water mass, this result might be important for the interpretation of paleoclimatic data.

The same qualitative behaviour was found by Bi et al (2001) in coupled model simulations of a scenario with increasing atmospheric CO_2-concentrations. Simulations using a forced ocean model suggested a seesaw between the two overturning cells (Seidov et al 2001). A follow-up study with a coupled climate model (Seidov et al 2005) led to the opposite behaviour when performing the same experiments. Both results are reconcilable with the presented scaling if the density difference between the inflowing water masses (NADW and AABW) $\Delta\rho_G$ varied during the simulation which was not investigated in the studies.

Interestingly, the Paleoclimate Modeling Intercomparison Project (PMIP) found that the density contrast between AABW and NADW at their source region is a major controlling factor for the strength of the modern and glacial AMOC in coupled model simulations (Weber et al 2007). The change in $\Delta\rho_G$ from modern to glacial conditions varies, however, greatly among different models. In agreement with the presented scaling the five models which showed almost no variation of $\Delta\rho_G$ are the ones where the strength of both cells increased in LGM as compared to modern conditions. Further analysis of our scaling relations are needed to interpret the results for models with varying $\Delta\rho_G$.

Note that the simulations with CLIMBER-3α are far from perfect. First it should be kept in mind that surface wind stress was fixed to present day climatology and that the atmospheric component does not resolve any form of variability. The oceanic circulation reproduces some coarse features of real ocean, but has a number of deficiencies. For example, the strength of the upper cell is with $\sim$12 Sv too weak compared to observations (Ganachaud and Wunsch 2003; Talley et al 2003) and the entire overturning is too shallow. AABW does reach all the way north to the Greenland-Scotland-ridge and in the Southern hemisphere flows partially east of the mid-Atlantic ridge which should be the case only north of the equator. Meso-scale eddy transport is not resolved but parameterized following Gent and McWilliams (1990). The main result of this study is thus the scaling analysis and its qualitative rathern than quantitative measure. The results should be validated against paleo evidence and using simulations with models of varying complexity.

Note also that we assume that diapycnal mixing in the main pycnocline is small, which seems to be observed in the ocean. Strong mixing in the upper ocean could significantly change the results described here. If the buoyancy flux that sustains the meridional density gradient within the bottom cell originates from the surface because of strong mixing in the pycnocline, then the strength of the upper cell might actually play an opposite effect on M. In this case the buoyancy from the surface is transported away by the upper cell towards the Southern Ocean. Thus the stronger the upper cell, the weaker the buoyancy forcing of the bottom cell. This mechanism would counteract the effect described here. Since many climate models apply larger values of diapycnal or vertical diffusivity than is observed and used in our simulation, further investigation of the issue is needed.

As a consequence of weak mixing in the pycnocline, both our simulations and scalings show that the dynamics of the NADW cell differs fundamentally from that of the bottom cell. This is due to the different sources of potential energy. While the upper cell in simulations and scaling was driven by Southern Ocean wind stress, the bottom cell needs to be driven by mixing. Consequently, the relation between vertical extent and volume transport of the upper cell is consistent with a WBC with very little diffusion-driven upwelling within the basin, i.e. vertical extent increases along with volume transport. The upwelling within the bottom overturning circulation, on the other hand, is consistent with a vertical advection-diffusion-balance and therefore driven by mixing. Consequently, the vertical extent of the bottom cell H decreases with increasing volume transport M (equation (3)).

In the limit of very strong NADW inflow the properties of the bottom cell are merely a function of the density difference between the inflowing water masses $\Delta\rho_G$. These saturation relations $M_\infty(\Delta\rho_G)$ and $H_\infty(\Delta\rho_G)$ can be used as a scale for the bottom cell and provide a transformation formular for paleodata.

A Derivation of the Advection-Diffusion balance equation

In this section we give a derivation for equation (2) which reflects the vertical balance of eddy-diffusion and advection of density within the Atlantic bottom cell. Note that we seek an expression for the large scale relation between the overturning strength M and the densities within the bottom overturning cell. As in (Munk 1966) and (Munk and Wunsch 1998), we assume a local balance of the vertical terms of the equilibrium tracer equations and a linear dependence of density on both temperature and salinity as well as the same eddy-diffusivity for temperature and salinity to get

$$\kappa \cdot \partial_z^2 \rho = w \cdot \partial_z \rho \tag{11}$$

Note that in most of the ocean $\partial_z \rho \leq 0$ and $\partial_z^2 \rho \leq 0$ which yields, in regions where equation (11) is valid, an upwelling $w \geq 0$. For a

spatially constant coefficient of vertical mixing κ, we obtain a general solution

$$\rho(z) = \rho_{SOB} - \delta\rho_0 \cdot \int_0^{z/H} d\eta \; e^{I(H\cdot\eta)} \tag{12}$$

where $\delta\rho_0$ is a constant of integration and

$$I(H\cdot\eta) \equiv \int_0^{H\cdot\eta} dz' \; \frac{w(z')}{\kappa} \tag{13}$$

The integration interval starts at the center of the inflowing AABW branch where the density is defined as ρ_{SOB}. At the depth of the southward return flow of the bottom cell equation (12) becomes

$$\rho_{SOB} - \rho_b = \delta\rho_0 \int_0^1 d\eta \; e^{I(H\cdot\eta)} \tag{14}$$

The upwelling velocity w has a maximum value w_{max} at the center of the overturning cell. In order to obtain a scaling of the overturning strength and the density differences, let us focus on the specific functional form of $w(z)$. By changing integration variables in equation (13) we obtain

$$I(H\cdot\eta) = \int_0^{\eta} d\eta' \; \frac{H\cdot w(\eta'\cdot H)}{\kappa} = \frac{H\cdot w_{max}}{\kappa} \cdot \int_0^{\eta} d\eta' \; f(\eta')$$

Here $f(\eta') \equiv w(H\cdot\eta')/w_{max}$ is a dimensionless which describes the shape of $w(z)$ but not its scaling. Since $w \geq 0$, $I(H\eta)$ has a maximum at $\eta = 1$. In equation (15) this maximum appears in the exponential and therefore dominates the integral. By use of the saddle-knot approximation we can replace the integral by the value at the maximum of the exponent which leads to

$$\rho_{SOB} - \rho_b \approx \delta\rho_0 \cdot H \cdot \frac{w_{max}}{\kappa} \cdot C \tag{15}$$

The constant $C \equiv \int_0^1 d\eta \; f(\eta')$ depends only on the normalized functional form of $w(z)$. For a quadratic profile it is $C = 2/3$, for a fourth order polynomial $C = 4/5$. We do not use this parameter for tuning purposed but simply apply the limit of an infinite order polynomial, $C = 1$, which corresponds to a very sharp transition of the upwelling velocity. Assuming horizontally uniform w_{max}, an integration over the horizontal plane in the center of the cell yields equation (2).

B Details of the simulations with CLIMBER-3α

Starting from the pre-industrial equilibrium simulation of CLIMBER-3α (Montoya et al 2005) with background vertical diffusivity $\kappa = 0.1 \cdot 10^{-4} m^2\, s^{-1}$, we applied anomalous freshwater flux to the ocean surface in the Atlantic. In order to test the robustness of the mechanism we conducted two classes of experiments. We first conducted four experiments with anomalous freshwater flux of $-0.4, -0.2, -0.1$ and $0.1Sv$ in the tropical Atlantic (18.75°N to 18.75°S and from 11.25°W to the western Atlantic coast) which are shown as triangles in figures 5, 6 and 7. For these experiments, the freshwater flux was compensated by a negative flux in the tropical Pacific (7.5°N to 7.5°S and from 138.7°E to the American Pacific coast).

In the second class of experiments (plotted as solid dots in figures 5, 6 and 7) we prescribed the momentum flux at the surface of the ocean from the NCEP-NCAR reanalysis (Kalnay et al 1996) and applied an anomalous freshwater fluxes of $0.05, 0.075, 0.1$ and $0.15Sv$ directly to the convection site regions (52○N to 80°N by 48°W to 15°E, excluding regions of shallow water along the northern European coast at 52°N to 64°N by 12°W to 8°E and along the Greenland coast at 63°N to 72°N by 31°W to 22°W) without compensation. This set-up allows us to demonstrate the robustness of the mechanism and captures a larger range of NADW overturning strength. In order to assure quasi-equilibrium, all simulations where started from a control run with more than 4000 simulation years and were run for at least 3000 years with anomalous freshwater forcing. The strength of the upper overturning cell m was defined as the volume transport crossing the Atlantic from 33.75°N to 33.75°S. Due to the different physical nature of the Atlantic reverse bottom cell, its strength M was computed as the minimum of the stream function at 33.75°S. The vertical extent H of the return flow was diagnosed as half the difference between 5000m depth and the depth of the zero-line of the stream function at 18.75°S. The vertical extent of the upper cell h was defined as the distance between the zero-line of the stream function and its maximum at the same latitude, 18.75°S. The error-bars were obtained by taking minimum and maximum of the same heights between 33.75°S and the equator. These definitions were chosen to capture the conceptual ideas used in the theory.

Acknowledgements The work was funded by the Gary Comer foundation. We are grateful to Michael McCartner for useful advice on existing observational data.

References

Adkins JF, McIntyre K, Schrag DP (2002) The salinity, temperature, and $\delta^{18}O$ of the glacial deep ocean. Science 298:1769–1773

Bi D, Budd WF, Hirst AC, Wu X (2001) Collapse and reorganisation of the Southern Ocean overturning under global warming in a coupled model. Geophysical Research Letters 28(20):3927–3930

Boyle EA, Keigwin LD (1982) Deep circulation of the North Atlantic over the last 200,000 years: Geochemical evidence. Science 218:784–787

Brix H, Gerdes R (2003) North Atlantic Deep Water and Antarctic Bottom Water: Their interaction and influence on the variability of the global ocean circulation. Journal of Geophysical Research 108:4–17

Broecker WS, Peng TH, Trumbore S, Bonani G, Wolfli W (1990) The distribution of radiocarbon in the glacial ocean. Global Biogeochemical Cycles 4:103–117

Broecker WS, Sutherland S, Peng TH (1999) A possible 20th-century slowdown of Southern Ocean Deep Water Formation. Science 286:1132–1135

Curry WB, Duplessy JC, Labeyrie LD, Shackelton NJ (1988) Changes in the distribution of $\delta^{13}C$ of deep water ΣCO_2 between the last glaciation and the Holocene. Paleoceanography 3:317–341

Duplessy JC, Shackleton NJ, Fairbanks RG, Labeyrie L, Oppo D, Kallel N (1988) Deep water source variations during the last climatic cycle and their impact on the global deep water circulation. Paleoceanography 3:343–360

England M (1993) Representing the global-scale water masses in Ocean General Circulation Models. Journal of Physical Oceanography 23:1523–1552

Ganachaud A, Wunsch C (2002) Oceanic nutrient and oxygen transports and bounds on export production during the World Ocean Circulation Experiment. Global Biogeochemical Cycles 16(4):1057

Ganachaud A, Wunsch C (2003) Large-scale ocean heat and freshwater transports during the World Ocean Circulation Experiment. Journal of Climate 16:696–705

Ganopolski A, Rahmstorf S, Petoukhov V, Claussen M (1998) Simulation of modern and glacial climates with a coupled global model of intermediate complexity. Nature 391:351–356

Gent PR, McWilliams JC (1990) Isopycnal mixing in Ocean Circulation Models. Journal of Physical Oceanography 20:150–155

Gnanadesikan A (1999) A simple predictive model for the structure of the oceanic pycnocline. Science 283:2077–2079

Goodman PJ (1998) The role of North Atlantic Deep Water formation in an OGCM's ventilation and Thermohaline Circulation. Journal of Physical Oceanography 28:1759–1785

Gregg MC, Sanford TB, Winkel DP (2003) Reduced mixing from the breaking of internal waves in equatorial waters. Nature 422:513–515

Hall M, McCartney M, Whitehead J (1997) Antarctic Bottom Water flux in the equatorial western Atlantic. Journal of Physical Oceanography 27:1903–1926

Hasumi H, Suginohara N (1999) Effects of locally enhanced vertical diffusivity over rough bathymetry on the world ocean circulation. Journal of Geophysical Research 104:23,364–23,374

Hattermann T, Levermann A (2009) Response of Southern Ocean circulation to global warming may enhance basal ice shelf melting around Antarctica. Climate Dynamics (in press)

Hewitt CD, Stouffer RJ, Broccoli AJ, Mitchell JFB, Valdes PJ (2001) The effect of ocean dynamics in a coupled GCM simulation of the Last Glacial Maximum. Climate Dynamics 20(2-3):203–218

Hofmann M, Maqueda MAM (2006) Performance of a second-order moments advection scheme in an Ocean General Circulation Model. Journal of Geophysical Research 111:C05,006

Kalnay E, Kanamitsu M, Kistler R, Collins W, Deaven D, Gandin L, Iredell M, Saha S, White G, Woollen J, Zhu Y, Chelliah M, Ebisuzaki W, Higgins W, Janowiak J, Mo KC, Ropelewski C, Wang J, Leetmaa A, Reynolds R, Jenne R, Joseph D (1996) The NCEP/NCAR 40-year reanalysis project. Bulletin of the American Meteorological Society 77:437–471

Kamenkovich IV, Goodman PJ (2000) The dependence of AABW transport in the Atlantic on vertical diffusivity. Geophysical Research Letters 27(22):3739–3742

Kitoh A, Murakami S, Koide H (2001) A simulation of the last glacial maximum with a coupled atmosphere-ocean GCM. Geophysical Research Letters 28:2221–2224

Kuhlbrodt T (2008) On Sandström's inferences from his tank experiments: a hundred years later. Tellus 60A:819–836

Kuhlbrodt T, Griesel A, Montoya M, Levermann A, Hofmann M, Rahmstorf S (2007) On the driving processes of the Atlantic meridional overturning circulation. Reviews of Geophysics 45:RG2001

Laurent LCS, Toole JM, Schmitt LC (2001) Buoyancy forcing by turbulence above rough topography in the abyssal Brazil Basin. Journal of Physical Oceanography 31:3476–3495

Ledwell JR, Watson AJ, Law CS (1993) Evidence for slow mixing across the pycnocline from an open-ocean tracer-release experiment. Nature 364:701–103

Ledwell JR, Watson AJ, Law CS (1998) Mixing of tracer in the pycnocline. Journal of Geophysical Research 103:21,499–21,529

Ledwell JR, Montgomery ET, Polzin KL, Schmitt LC, Toole JM (2000) Evidence for enhanced mixing over rough topography in the abyssal ocean. Nature 403:179–182

Levermann A, Griesel A, Hofmann M, Montoya M, Rahmstorf S (2005) Dynamic sea level changes following changes in the thermohaline circulation. Climate Dynamics 24:347–354

Levermann A, Mignot J, Nawrath S, Rahmstorf S (2007) The role of northern sea ice cover for the weakening of the thermohaline circulation under global warming. Journal of Climate 20:4160–4171

Limeburner R, Whitehead JA, Cenedese C (2005) Variability of Antarctic Bottom Water flow into the North Atlantic. Deep-Sea Research II 52:495–512

Luyten J, McCartney MS, Stommel H, Dickson R, Gmitrowicz E (1993) On the sources of North Atlantic Deep Water. Journal of Physical Oceanography 23:1885

Mauritzen C, Polzin KL, McCartney MS, Millard RC, West-Mack DE (2002) Evidence in hydrography and density fine structure for enhanced vertical mixing over the Mid-Atlantic Ridge in the western Atlantic. Journal of Geophysical Research 107 C10:3147, DOI 10.1029/2001JC001114

McCartney MS, Talley LD (1984) Warm-to-cold conversion in the northern North Atlantic ocean. Journal of Physical Oceanography 14:922–935

Mignot J, Levermann A, Griesel A (2006) A decomposition of the Atlantic meridional overturning circulation into physical components using its sensitivity to vertical diffusivity. Journal of Physical Oceanography 36:636–650

Molinari R, Fine R, Johns E (1992) The deep western boundary current in the tropical North Atlantic ocean. Deep-Sea Research 39:1967–1984

Montoya M, Levermann A (2008) Surface wind-stress threshold for glacial Atlantic overturning. Geophysical Research Letters 35:DOI:10.1029/2007GL032,560

Montoya M, Griesel A, Levermann A, Mignot J, Hofmann M, Ganopolski A, Rahmstorf S (2005) The Earth System Model of Intermediate Complexity CLIM*BER*-3α. Part I: description and performance for present day conditions. Climate Dynamics 25:237–263

Moum J, Osborn T (1986) Mixing in the main thermocline. Journal of Physical Oceanography 16:1250–1259

Moum J, Caldwell D, Nash J, Gunderson G (2002) Observations of boundary mixing over the continental slope. Journal of Physical Oceanography 32:2113–2130

Munk W (1950) On the wind-driven ocean circulation. J Meteorol 7:80–93

Munk W (1966) Abyssal recipes. Deep-Sea Research 13:707–730

Munk W, Wunsch C (1998) Abyssal recipes II. Deep-Sea Research I 45:1977–2010

Murray R, Reason CJ (1999) Influences of topography in the modeling of abyssal water masses. Part I: effects of channel representation. Journal of Physical Oceanography 29:2851–2871

Oakey N, Ruddick B, Walsh D, Burke J (1994) Turbulence and microstructure measurements during NATRE. EOS 75:130

Otto-Bliesner B, Hewitt C, Marchitto T, Brady E, Abe-Ouchi A, Crucifix M, Murakami S, Weber S (2007) Last glacial maximum ocean thermohaline circulation: Pmip2 model intercomparisons and data constraints. Geophysical Research Letters 34(L12706), DOI 10.1029/2007GL029475

Polzin KL, Toole JM, Ledwell JR, Schmitt RW (1997) Spatial variability of turbulent mixing in the abyssal ocean. Science 276:93–96

Prather MJ (1986) Numerical advection by conservation of second-order moments. Journal of Geophysical Research 91:6671–6681

Rahmstorf S (1996) On the freshwater forcing and transport of the Atlantic thermohaline circulation. Climate Dynamics 12:799–811

Rahmstorf S (2002) Ocean circulation and climate during the past 120,000 years. Nature 419:207–214

Reid JL (1989) On the total geostrophic circulation of the South Atlantic Ocean: flow patterns, tracers and transports. Progress in Oceanography 23:149

Rhein M, Stramma L, Krahmann G (1998) The spreading of Antarctic Bottom Water in the tropical Atlantic. Deep-Sea Research I 45:507–527

Sandström JW (1908) Dynamische Versuche mit Meerwasser. Annalen der Hydrographie und Maritimen Meteorologie pp 6–23

Schewe J, Levermann A (2009) The role of meridional density differences for a wind-driven overturning circulation. Climate Dynamics DOI 10.1007/s00382-009-0572-1

Seidov D, Barron E, Haupt BJ (2001) Meltwater and the global ocean conveyor: northern versus southern connections. Global and Planetary Change 30:257–270

Seidov D, Stouffer RJ, Haupt BJ (2005) Is there a simple bi-polar ocean seesaw? Global and Planetary Change 49:19–27

Shin SI, Liu Z, Otto-Bliesner BL, Kutzbach JE, Vavrus SJ (2003) Southern Ocean sea-ice control of the glacial North Atlantic thermohaline circulation. Geophysical Research Letters 30:68–1

Sloyan BM, Rintoul SR (2000) Estimates of area-averaged diapycnal fluxes from basin-scale budgets. Journal of Physical Oceanography 30:2320–2341

Smethie WM, Fine R, Putzka A, Jones E (2000) Tracing the flow of North Atlantic Deep Water using chlorofluorocarbons. Journal of Geophysical Research 105(C6):14,297–14,323

Stommel H (1961) Thermohaline convection with two stable regimes of flow. Tellus 13:224–230

Talley LD, Reid JL, Robbins PE (2003) Data-based meridional overturning streamfunctions for the global ocean. Journal of Climate 16:3213–3226

Toggweiler JR, Samuels B (1998) On the ocean's large scale circulation in the limit of no vertical mixing. Journal of Physical Oceanography 28:1832–1852

Toole JM, Polzin KL, Schmitt RW (1994) Estimates of diapycnal mixing in the abyssal ocean. Science 264:1120–1123

Weatherly GL, Kim YY, Kontar EA (2000) Eulerian measurements of the North Atlantic Deep Water Deep Western Boundary Current at 18°S. Journal of Physical Oceanography 30:971–986

Weber S, Drijfhout S, Abe-Ouchi A, Crucifix M, Eby M, Ganopolski A, Murakami S, Otto-Bliesner B, Peltier W (2007) The modern and glacial overturning circulation in the Atlantic ocean in PMIP coupled model simulations. Climate of the Past, 3(1):51–64

Whitehead JA, Worthington L (1982) The flux and mixing rates of Antarctic Bottom Water within the North Atlantic. Journal of Geophysical Research 87:7903

Wright DG, Stocker TF, Mercer D (1998) Closures used in zonally averaged ocean models. Journal of Physical Oceanography 28:791–804

Wunsch C, Ferrari R (2004) Vertical mixing, energy and the general circulation of the oceans. Annual Reviews of Fluid Mechanics 36:281–314